CHAPTER 6

MODELING OF COMPOSITE POWER SYSTEMS

The stability problem in a power system is principally one of keeping the interconnected synchronous generators in synchronism and damping rotor oscillations following a system disturbance. Therefore, accurate modeling of synchronous generators is of fundamental importance for off–line simulation studies related to the problem. A synchronous generator includes three parts; namely, a generating unit, an excitation system, and a speed–governing and turbine system. Synchronous generators are interconnected through an AC/DC transmission network to which various loads, such as induction motors, are connected as the end users of electrical energy. This chapter discusses the modeling aspect of these devices.

6.1 INTRODUCTION

The study of transient stability of a power system is concerned with the investigation of changing phenomena of electric quantities when the operating environment of the system is disturbed. To carry out such an investigation, power apparatuses must be modeled using mathematical expressions in computer simulations. They include synchronous machines, transformers, transmission lines, and loads. Synchronous machines play a

vital role in a power system. Synchronous generators convert mechanical energy into electric energy. Synchronous motors drive loads and convert electric energy to mechanical energy. Synchronous condensers generate reactive power into the system to improve voltage profiles. Transformers and transmission lines are equipment indispensable in transporting electric energy from the source to the point of consumption. Electric loads are variables that change over time. The principal task of the power system is to continuously match the electric energy supply to these changing loads, which gives rise to the problem of stability.

Large power systems consist of many local power systems connected through long transmission lines. In special situations, such connections may not be possible by using AC transmission. For example, two AC systems with different operating frequencies can not be connected with an AC link. In such situations high–voltage direct–current (HVDC) transmission has to be used.

6.2 MODELING OF POWER COMPONENTS

6.2.1 Synchronous Machines

The actual structure of a synchronous machine is complicated. Magnetically it is equivalent to many windings coupled together. The synchronous machine under study is assumed to have three identical, symmetrically placed stator windings, one field winding and two amortisseur or damper windings. All

these windings are magnetically coupled, depending on the position of the rotor. Therefore the flux linking each winding is a function of the rotor position.

The mathematical description of the machine is very complicated as it consists of both stationary and rotational parts. Park transformation is usually used to simplified this description[6–1].

This transformation projects the original variables onto a rotational coordinate system called the $d-q-0$ system. When this transformation is performed, the flux equations of the numerous axes become linear functions of currents flowing in the stator and damper windings. A pictorial representation of the synchronous machine is given in Figure 6.1. Assume that positive stator currents i_d and i_q are generated currents, positive rotor currents i_f, i_D, and i_Q flow into the machine, where d, q, f, D and Q denote the direct–axis stator winding, quadrature–axis stator winding, and the field winding, the direct–axis and quadrature–axis damper windings. The voltage equations of the various windings are listed below, with transformer voltages ignored,

$$v_d = -\frac{d}{dt}\left(\phi_q\right) - r_a i_d \tag{6.1}$$

$$v_q = \frac{d}{dt}\left(\phi_d\right) - r_a i_q \tag{6.2}$$

$$\frac{d}{dt}\left(\phi_f\right) = v_f - r_f i_f \tag{6.3}$$

Fig. 6.1 Pictorial Representation of A Synchronous Machine

$$\frac{d}{dt}\left(\phi_D\right) = -r_D i_D \tag{6.4}$$

$$\frac{d}{dt}\left(\phi_Q\right) = -r_Q i_Q \tag{6.5}$$

where,

v = the voltage,

r = the resistance, and

ϕ = the flux linkage of a winding.

The flux linkage is determined by the following equation, accordingly,

$$\phi_d = -x_d i_d + x_{ad} i_f + x_{ad} i_D \tag{6.6}$$

$$\phi_f = -x_{ad} i_d + x_f i_f + x_{fD} i_D \tag{6.7}$$

$$\phi_D = -x_{ad} i_d + x_{fD} i_f + x_D i_D \tag{6.8}$$

$$\phi_q = -x_q i_q + x_{aq} i_Q \tag{6.9}$$

$$\phi_Q = -x_{aq} i_q + x_Q i_Q \tag{6.10}$$

where,

x_d, x_q, x_{fD}, x_D and x_Q are complete reactance,

x_{ad} and x_{aq} are mutual reactance, and

$x_{fD} = x_{ad}$.

Solving (6.6) ~ (6.8) for ϕ_d expressed in terms of ϕ_f, ϕ_D and i_d, we have

$$\begin{aligned} \phi_d &= \frac{x_{ad}}{x_D x_f - x_{ad}^2}\left\{\left(x_D - x_{ad}\right)\phi_f + \left(x_f - x_{ad}\right)\phi_D\right\} \\ &\quad - \left\{x_d - \frac{x_{ad}^2\left(x_D + x_f - 2x_{ad}\right)}{x_D x_f - x_{ad}^2}\right\} i_d \end{aligned} \tag{6.11}$$

Defining the $q-$axis subtransient voltage as,

$$E_q'' = \frac{x_{ad}}{x_D x_f - x_{ad}^2}\left\{\left(x_D - x_{ad}\right)\phi_f + \left(x_f - x_{ad}\right)\phi_D\right\} \tag{6.12}$$

and subtransient reactance as,

$$x_d'' = \left\{x_d - \frac{x_{ad}^2\left(x_D + x_f - 2x_{ad}\right)}{x_D x_f - x_{ad}^2}\right\} \tag{6.13}$$

Then the voltage equation of (6.2) can be rewritten as,

$$v_q = E_q'' - x_d'' i_d - r_a i_q \tag{6.14}$$

Similarly, defining the $d-$axis subtransient voltage and reactance as,

$$E_d^{''} = -\frac{x_{aq}}{x_Q}\phi_Q \tag{6.15}$$

$$x_q^{''} = x_q - \frac{x_{aq}^2}{x_Q} \tag{6.16}$$

Then the voltage equation of (6.1) on $d-$axis can be rewritten as

$$v_d = E_d^{''} + x_q^{''} i_q - r_a i_d \tag{6.17}$$

A block diagram for this model is shown in Figure 6.2.

(a) *Two–Axes Model with Subtransient*

In this model, the damping effect of the rotor is represented by two short–circuited damper windings. The following derived differential equations are utilized to describe the subtransient behavior of a synchronous machine (see Appendix A for detailed derivation):

$$\frac{d}{dt}\left(E_q^{'}\right) = \frac{1}{\tau_{do}^{'}}\left\{kE_{fd} - E_q^{'} - \left(x_d - x_d^{'}\right)i_d\right\} \tag{6.18}$$

$$\frac{d}{dt}\left(E_{sum}\right) = \frac{1}{\tau_{do}^{''}}\left\{-E_{sum} - \left(x_d^{'} - x_d^{''}\right)i_d\right\} \tag{6.19}$$

$$\frac{d}{dt}\left(E_d^{''}\right) = \frac{1}{\tau_{qo}^{''}}\left\{-E_d^{''} + \left(x_q - x_q^{''}\right)i_q\right\} \tag{6.20}$$

where $E_{sum} = E_q^{''} - E_q^{'}$.

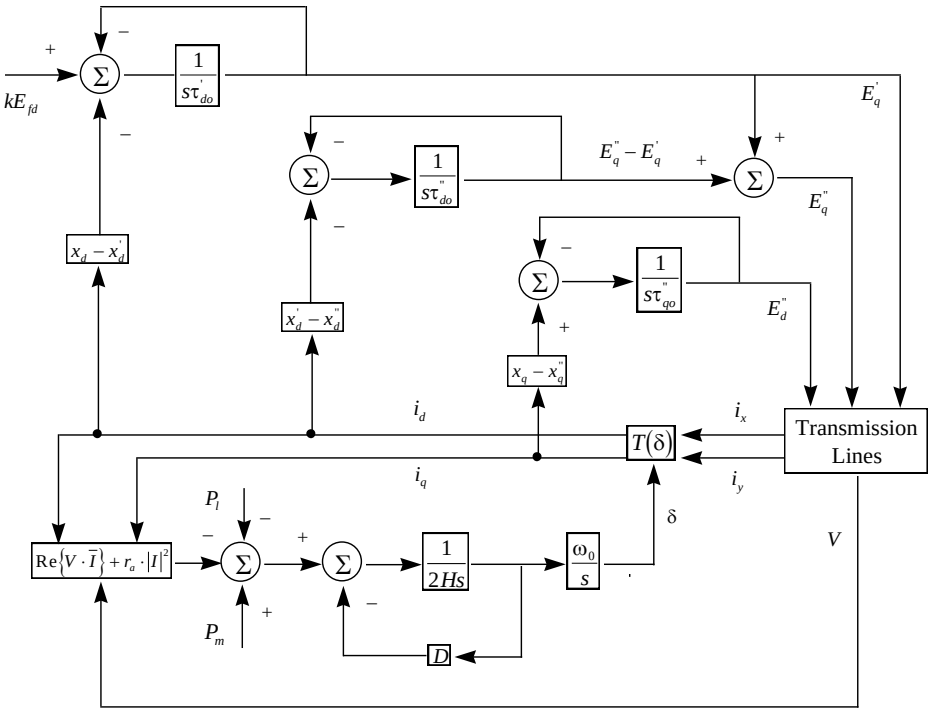

Fig. 6.2 Block Diagram of the Synchronous Generator Model

The differential equation describing machine motion is given by

$$\frac{d^2\delta}{dt^2} = (P_m - P_e - P_l - D\Delta\omega)/2H \tag{6.21}$$

$$\frac{d\delta}{dt} = \omega_0(\Delta\omega) \tag{6.22}$$

where

H = the machine inertia constant in seconds,

P_m = the mechanical power input to the generator,

P_e = the electrical power output from the generator to the system,

P_l = the power loss in the stator windings, and

ω_0 = the synchronous speed of the machine in radians per second.

Generator saturation can be taken into account by modifying the reactance x_{ad} and x_{aq} according to machine saturation at 1.0 per unit and 1.2 per unit terminal voltage that usually are known from the manufacturer. There are several algorithms to realize this modification [6–2,6–3]. An iterative procedure was employed in the studies reported in this thesis. At the same time, the corresponding time constants must also be modified. A detailed derivation of these expressions is given in Appendix. The equations are included here to maintain completeness of the mathematical model of the synchronous machine modeled by the two–axis representation with subtransient. The saturated time constants are modified as follows:

$$\tau'_{do} = \tau'^{(0)}_{do}\left\{k + (1-k)\frac{x'_d - x_l}{x_d^{(0)} - x_l}\right\} \tag{6.23}$$

$$\tau''_{do} = \tau''^{(0)}_{do}\left\{k + (1-k)\frac{x''_d - x_l}{x_d^{(0)} - x_l}\right\} \tag{6.24}$$

$$\tau''_{qo} = \tau''^{(0)}_{qo}\left\{k + (1-k)\frac{x''_q - x_l}{x_q^{(0)} - x_l}\right\} \tag{6.25}$$

where the superscript (0) indicates unsaturated values, and k is the saturation factor. Other symbols are listed at the beginning of this thesis.

The interface between the generator model and the terminal of the transmission network is accomplished by the following two equations.

$$v_q = E''_q - x''_d i_d - r_a i_q \tag{6.26}$$

$$v_d = E''_d + x''_q i_q - r_a i_d \tag{6.27}$$

(b) *Two–Axis Model with Transient*

This model is similar to the one presented previously. The subtransient effects are totally ignored, however, the transient effects are taken into account. There are two rotor windings, one is the field winding in the $d-$axis and the other is the equivalent damper winding in the $q-$axis formed by the solid rotor. The basic equations of this model are given by:

$$v_q = E_q^{'} - x_d^{'} i_d - r_a i_q \tag{6.28}$$

$$v_d = E_d^{'} + x_q^{'} i_q - r_a i_d \tag{6.29}$$

$$\frac{d}{dt}\left(E_q^{'}\right) = \frac{1}{\tau_{do}^{'}}\left\{kE_{fd} - E_q^{'} - \left(x_d - x_d^{'}\right)i_d\right\} \tag{6.30}$$

$$\frac{d}{dt}\left(E_d^{'}\right) = \frac{1}{\tau_{qo}^{'}}\left\{-E_d^{'} + \left(x_q - x_q^{'}\right)i_q\right\} \tag{6.31}$$

where $\tau_{do}^{'}$ is modified according to (6.24); and

$$\tau_{qo}^{'} = \tau_{qo}^{'(0)}\left\{k + (1-k)\frac{x_q^{'} - x_l}{x_q^{(0)} - x_l}\right\}. \tag{6.33}$$

(c) *One–Axis Model with Transient*

In this model, the amortisseur effects are totally neglected. There is only one rotor winding present in the model, i.e., the field winding. Its differential equation is given by (6.34). Saturation is treated in the same manner as explained previously. The difference between this model and the two–axis transient model is that as no damper windings are modeled, the differential equation for $E_d^{'}$ is, therefore, eliminated.

$$\frac{d}{dt}\left(E_q^{'}\right)=\frac{1}{\tau_{do}^{'}}\left\{kE_{fd}-E_q^{'}-\left(x_d-x_d^{'}\right)i_d\right\} \tag{6.34}$$

(d) *Infinite–Bus Model*

To accommodate a large power system in computer simulation studies, it is often necessary that part of the system be modeled as an infinite–bus which generates or absorbs large amount of power and at the same time maintains constant terminal voltage. Details on how this is done will be given in Chapter 7.

6.2.2 Excitation Systems

Since the 1960s, excitation systems have been represented in extra detail in transient stability programs, thanks to the availability of economic computing power. A 1968 IEEE report reviewed the computer representation of excitation systems available at the time[6–4]. In 1981, IEEE published standard excitation models used in the power industry[6–5]. In 1992, IEEE Standard 421.5, "IEEE Recommended Practice for Excitation System Models for Power System Stability Studies" was adopted[6–6]. These models are also used in TSSP software[6–7]. In recent years, there have been many new excitation systems applied. Most of the new systems have digital–based controls, that is, they use microprocessor technology to implement the control algorithms. These digital–based controls offer flexibility and control options that are difficult to implement in analog control systems.

Standard analog excitation systems are listed in [6–5, 6–6] and user–defined models can be incorporated in the TSSP software[6–7]. Some variations of these standard models are presented in[6–8]. In this section, we present two analog and one digital excitation system. Figure 6.3 shows the block diagram of an analog excitation system, referred as DC Type 1 excitation system[6–5], where $V_{err} = V_{ref} - V_t$; V_s is the output signal from a power system stabiliser.

Figure 6.4 shows the general structure of a digital excitation system. It consists of the digital part and the interface A/D and D/A converters as included in the dashed–line box. The output of the generator is sensed and scaled down to appropriate levels and converted into digital words by the A/D converter. It is then compared with the reference input that is held in the RAM of the microprocessor. The result is acted upon by a controller that can realize classical control algorithms such as PID control and newer schemes such as fuzzy logic and adaptive control. Apart from the common features available in both analog and digital excitation systems, the latter can be designed to implement extremely sophisticated control algorithms such as transient gain reduction, power system stabilizer(PSS) control, Var/power factor control, under/over excitation limit control, stator current limit control and many other features[6–8]. Digital systems are relatively immune to parameter changes. They provide increased accuracy and precision.

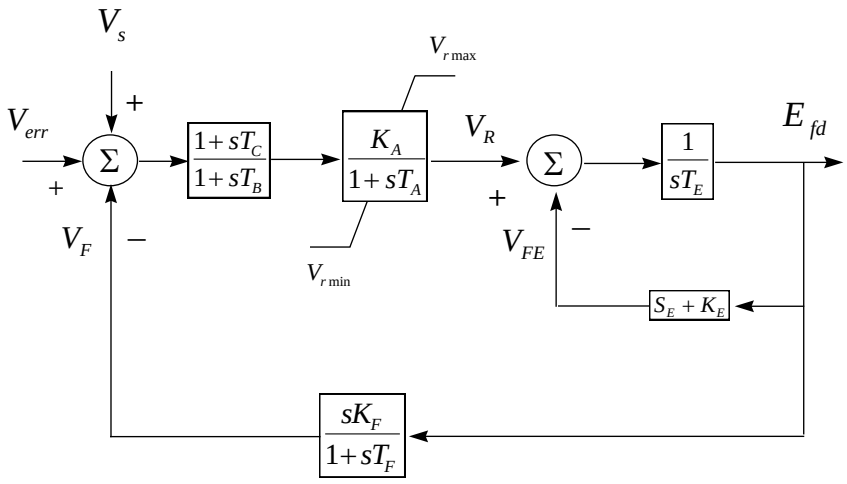

Fig. 6.3 Block Diagram of DC Type 1 Excitation System[6–5]

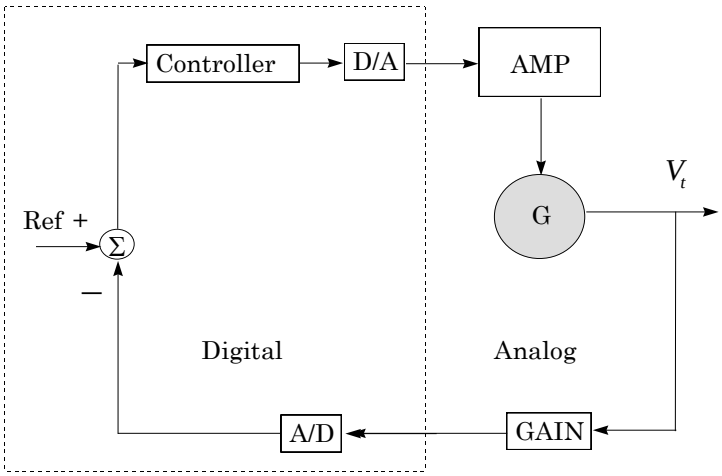

Fig. 6.4 Block Diagram of A Digital Excitation System

Shown in Figure 6.5 is an alternator–rectifier excitation system. It represents the Basler DECS voltage regulator as applied to a brushless exciter[6–6]. The AVR in this model consists of PID control. The values for the proportional, integral, and derivative gains are chosen for best performance from each particular generator excitation system. Other excitation models will be further covered in Chapter 7 where TSSP in SIMULINK is presented.

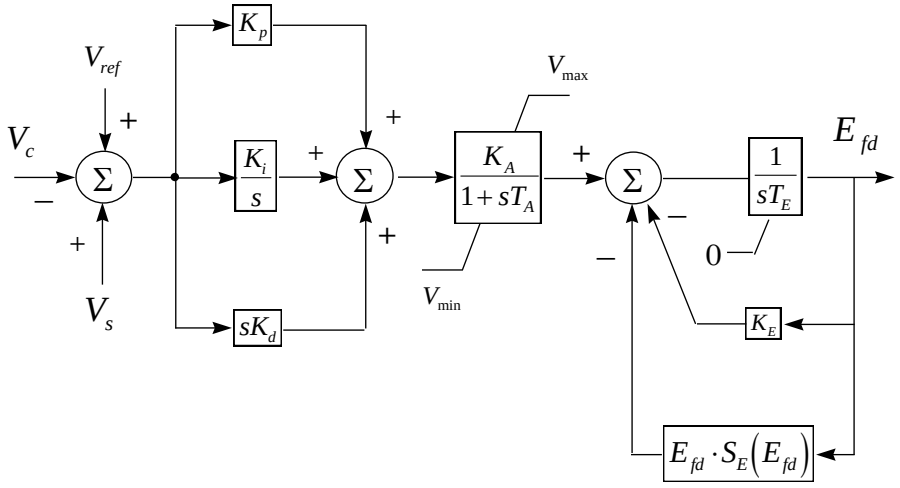

Fig. 6.5 Alternator–Rectifier Excitation System[6–6]

6.2.3 PRIME MOVERS

Electrical energy is converted from mechanical energy by synchronous generators. The prime mover governing system provides a means of controlling the input of mechanical energy to the generator so that the generated power and its frequency can be controlled. This prime mover includes speed–governing and turbine system for both steam and hydro generators. In this section, we discuss both hydro and steam turbines and governing systems. For detailed description of these systems, the reader is referred to [6–10].

There are two types of speed governing systems for hydroturbines, i.e., mechanical–hydraulic control and electric–hydraulic control. As the dynamic performance of the electric governor is necessarily adjusted to be the same as that of the mechanical governor for interconnected system operation, only one single model is needed[6–11]. Figure 6.6 shows the detailed model of a hydro–turbine and speed governing system. Figure 6.7 shows its equivalent representation. Their simulation models will be discussed in Chapter 7.

Figure 6.8 shows a block diagram that may be used to represent either a mechanical–hydraulic system or an electric–hydraulic system for a steam turbine by selecting the parameters appropriately. In the model it is seen that P_0 is an initial load reference. Figure 6.9 shows the Tandem–Compound Double Reheat steam turbine system[6–11].

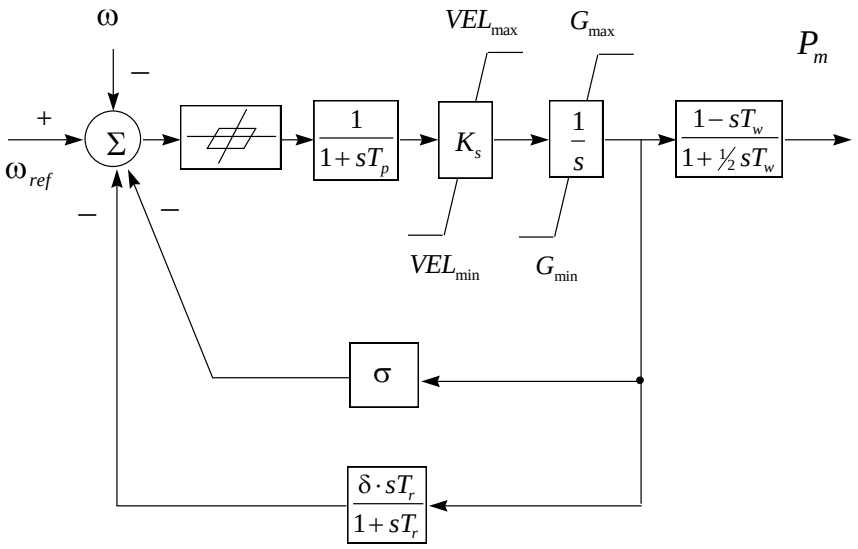

Fig. 6.6 Detailed Representation of Hydrogovernor Turbine System[6–11]

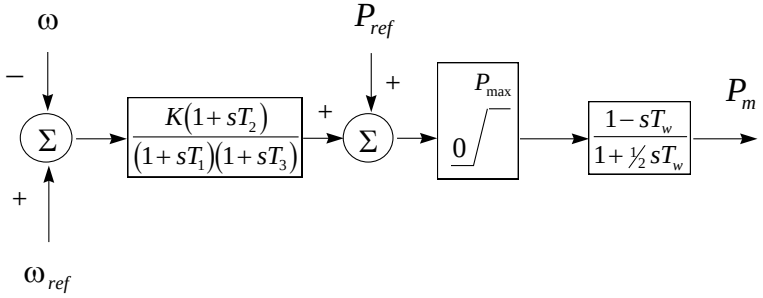

Fig. 6.7 Equivalent Representation of Hydrogovernor Turbine System[6–11]

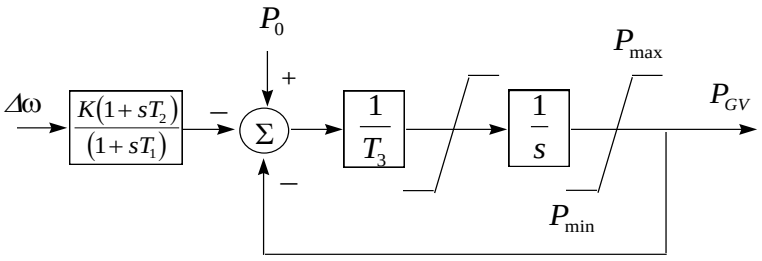

Fig. 6.8 Speed Governing System for Steam Turbines[6–11]

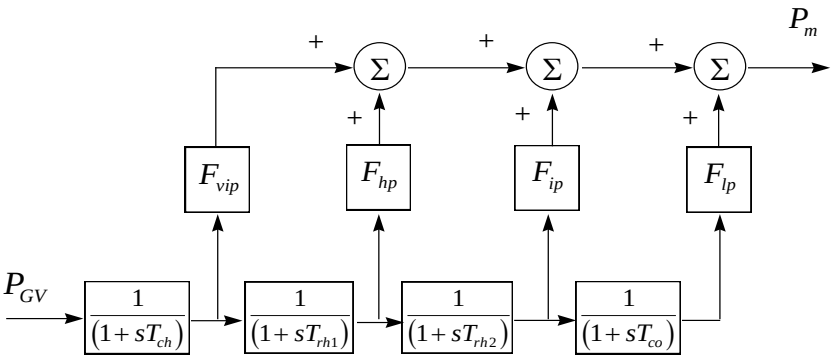

Fig. 6.9 Block Diagram of A Steam Turbine[6–11]

6.2.4 Conventional PSS

In order to suppress the low frequency electromechanical oscillations in a power system, supplementary excitation controllers known as power system stabilizers(PSSs) are often installed to provide positive damping [6–12]. The block diagram of the IEEE standard PSS model[6–5] is shown in Figure 6.10. The transfer function of the filter in the diagram can be expressed by

$$\frac{1+A_5 s+A_6 s^2}{\left(1+A_1 s+A_2 s^2\right)\left(1+A_3 s+A_4 s^2\right)} \tag{6.35}$$

The input signal to a PSS can be arbitrary. Generally, any one or a combination of the following can be utilized as input signal. (a) deviation of machine shaft speed; (b) deviation of terminal frequency; (c) net accelerating power; (d) deviation of terminal voltage.

The input signals must be in per unit. A PSS with a different input signal will have a different transfer function. Two specific PSS models are used in the studies reported in this thesis. Their input signals are generator electrical power and net accelerating power, respectively. The former is identified as IEEEST and the latter as IEEESN. Their block diagrams are shown in Figure 6.11 and Figure 6.12, respectively.

Note that only a single time constant A_1 is present in the filter transfer function in Figs. 6.11 and 6.12. This is because of the inherently low level of torsional interaction when net accelerating power is used as stabilizer input.

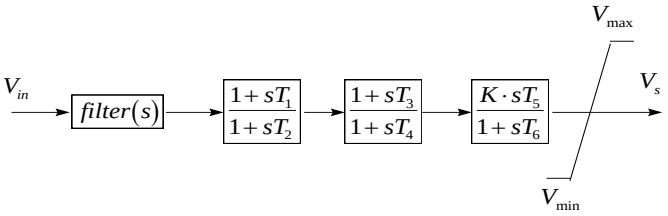

Fig. 6.10 IEEE Standard PSS Model[6–12]

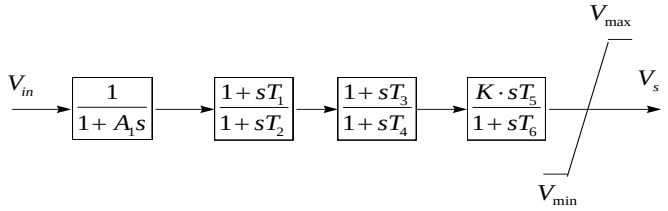

Fig. 6.11 IEEEST PSS Using Net Accelerating Power As Input[6–5]

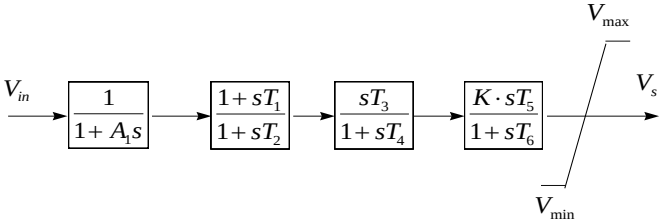

Fig. 6.12 IEEE PSS Using Generated Electric Power As Input[6–5]

6.2.5 POWER SYSTEM LOADS

Appropriate representation of power system loads in transient stability studies is important as loads have a great influence on system stability. On the other hand, the modeling of loads is a complicated issue as there are so many loads in a system and at each bus the load composition is different and most of the time is unknown. Moreover, this composition changes over time. Therefore, simplification and certain assumptions have to be used in representing each load. In [6–13], IEEE has presented the state of the art of representation of power system loads for dynamic performance analysis in practice today. In this section, we present the most frequently used load models in transient stability studies. Detailed modeling of large induction motors is also given [6–14].

(1) *Constant Impedance Model*

In this model, the power varies directly with the square of the voltage magnitude, i.e.,

$$P + jQ = \left(\frac{1}{Z}\right) \cdot V^2 \tag{6.36}$$

(2) *Constant Current Model*

In this model, the power varies directly with the voltage magnitude, i.e.,

$$P + jQ = V \cdot \bar{I} \tag{6.37}$$

(3) *Constant Power Model*

In this model, the power does not vary with the changes in voltage magnitude. It may also be called constant MVA load model.

(4) *Polynomial Load Model*

This model expresses the relationship between power and voltage magnitude as:

$$P = P_0\left\{a_1\left(V/V_0\right)^2 + a_2\left(V/V_0\right) + a_3\right\} \tag{6.38}$$

$$Q = Q_0\left\{a_4\left(V/V_0\right)^2 + a_5\left(V/V_0\right) + a_6\right\} \tag{6.39}$$

where

V_0 = the rated voltage,

P_0 = the active power consumed at rated voltage;

Q_0 = the reactive power consumed at rated voltage.

However, these values are normally taken as the values at the initial system operating condition for the study. The coefficients in the model satisfy the following equations[6–13]:

$$a_1 + a_2 + a_3 = 1 \tag{6.40}$$

$$a_4 + a_5 + a_6 = 1 \tag{6.41}$$

6.2.6 Induction Motors

Representation of induction motors for transient stability studies can be derived following similar procedures as used in deriving synchronous machine models. The final model can be expressed in the $d-q-0$ reference frame. As the rotor of an induction motor has a symmetrical structure, its equivalent circuit on $d-$axis, and $q-$axis will be the same. The dynamics of the rotor circuits are determined by the slip that changes with the loading. In this section, we present detailed modeling of induction motors. The material that follows logically belongs to the section of power system loads. The present arrangement emphasizes its importance and uniqueness as compared with other loads.

For a three–phase induction motor, the number of poles of the field produced by the induced rotor currents is the same as that of the field produced by the stator winding. Therefore the rotor can be modeled by an equivalent three–phase winding. The rotor may be constructed in one of two ways, i.e., one with wound rotor where conventional three–phase windings are brought out through three slip rings on the shaft and connected to external circuits; the other with squirrel–cage rotor which consists of a number of bars short–circuited by end rings at both ends.

Choose the $d-q-0$ reference frame with its axes rotating at the synchronous speed. The $q-$axis is 90° ahead of the $d-$axis in the direction of rotation. Let the $d-$axis coincide with the phase $a-$axis at time $t \geq 0$. As

indicated in Figure 6.13, its displacement from phase $a-$axis at any time t is $\omega_s t$, where ω_s is the angular velocity of the stator field in electrical radians per second.

Let subscript s denote quantities of the stator and r of the rotor. The mathematical equations of an induction motor in per unit in the $d-q-0$ reference frame, can be summarized as follows[6–10]:

Stator voltage:

$$v_{ds} = R_s i_{ds} - \omega_s \phi_{qs} \tag{6.42}$$

$$v_{qs} = R_s i_{qs} + \omega_s \phi_{ds} \tag{6.43}$$

Rotor voltages:

$$v_{dr} = R_r i_{dr} - \frac{d}{dt}(\theta_r)\phi_{qs} + \frac{d}{dt}(\phi_{dr}) \tag{6.44}$$

$$v_{qr} = R_r i_{qr} + \frac{d}{dt}(\theta_r)\phi_{ds} + \frac{d}{dt}(\phi_{qr}) \tag{6.45}$$

Flux linkages:

$$\phi_{ds} = L_{ss} i_{ds} + L_m i_{dr} \tag{6.46}$$

$$\phi_{qs} = L_{ss} i_{qs} + L_m i_{qr} \tag{6.47}$$

$$\phi_{dr} = L_m i_{ds} + L_{rr} i_{dr} \tag{6.48}$$

$$\phi_{qr} = L_m i_{qs} + L_{rr} i_{qr} \tag{6.49}$$

where

$L_{ss} = L_s + L_m$,

$L_{rr} = L_r + L_m$,

Fig. 6.13 Induction Motor

L_s , L_r = stator and rotor leakage inductances, respectively,

L_m = mutual inductance, and

ϕ = the flux linkage.

All the quantities are in per unit. Eliminating the rotor currents, we have from (6.48),

$$i_{dr} = \frac{\phi_{dr} - L_m i_{ds}}{L_{rr}} \tag{6.50}$$

Substituting (6.50) into (6.46), we have

$$\phi_{ds} = L_{ss} i_{ds} + \frac{L_m \left(\phi_{dr} - L_m i_{ds} \right)}{L_{rr}}$$

$$= \frac{L_m}{L_{rr}}\phi_{dr} + \left(L_{ss} - \frac{L_m^2}{L_{rr}}\right) i_{ds} \tag{6.52}$$

Substituting (6.52) into (6.43), we have

$$v_{qs} = R_s i_{qs} + \omega_s \frac{L_m}{L_{rr}}\phi_{dr} + \omega_s \left(L_{ss} - \frac{L2_m}{L_{rr}}\right) i_{ds}$$

$$= R_s i_{qs} + x_s^{'} i_{ds} + E_q^{'} \tag{6.53}$$

where

$$E_q^{'} = \omega_s \frac{L_m}{L_{rr}}\phi_{dr},$$

$x_s^{'} = \omega_s \left(L_{ss} - \frac{L_m^2}{L_{rr}}\right)$, transient reactance of the induction machine.

Similarly, for the d –axis,

$$v_{ds} = R_s i_{ds} - x_s^{'} i_{qs} + E_d^{'} \tag{6.54}$$

where

$$E_d^{'} = -\omega_s \frac{L_m}{L_{rr}}\phi_{qr}.$$

From (6.48) and (6.49), we derive the differential equations for $E_d^{'}$ and $E_q^{'}$.

$$\frac{dE_q^{'}}{dt} = \omega_s \frac{L_m}{L_r}\frac{d}{dt}\left(\phi_{dr}\right)$$

$$= \omega_s \frac{L_m}{L_{rr}}\left[-R_r i_{dr} + \frac{d}{dt}\left(\theta_r\right)\phi_{qr}\right]$$

$$= -\omega_s \frac{L_m}{L_{rr}}\left[\frac{\phi_{dr} - L_m i_{ds}}{L_{rr}}\right] + \omega_s \frac{L_m}{L_{rr}}\frac{d}{dt}\left(\theta_r\right)\phi_{qr}$$

$$= -\frac{1}{\tau_o^{'}}\left[E_q^{'} - \omega_s \frac{L_m^2}{L_{rr}} i_{ds}\right] + \omega_s \frac{L_m}{L_{rr}} \frac{d}{dt}(\theta_r)\phi_{qr}$$

$$= -\frac{1}{\tau_o^{'}}\left[E_q^{'} - \left(x_s - x_s^{'}\right) i_{ds}\right] - E_d^{'} \frac{d}{dt}(\theta_r) \tag{6.55}$$

where

$$\left(x_s - x_s^{'}\right) = \omega_s \frac{L_m^2}{L_{rr}}.$$

Similarly,

$$\frac{dE_d^{'}}{dt} = -\omega_s \frac{L_m}{L_r} \frac{d}{dt}\left(\phi_{qr}\right)$$

$$= -\frac{1}{\tau_o^{'}}\left[E_d^{'} + \left(x_s - x_s^{'}\right) i_{qs}\right] + E_q^{'} \frac{d}{dt}(\theta_r) \tag{6.56}$$

where

$$\tau_o^{'} = \frac{L_{rr}}{R_r},$$

$x_s = \omega_s L_{ss}$, and

$$\frac{d}{dt}(\theta_r) = \frac{\omega_s - \omega_r}{\omega_s}.$$

ω_s is the angular velocity of the rotor in radian per second. θ_r is the angle by which the $d-$axis leads phase $A-$axis of the rotor. If the rotor slip is s, the $d-$axis is advancing with respect to a point on the rotor at the rate

$$\frac{d}{dt}(\theta_r) = s \cdot \omega_s \tag{6.57}$$

The rotor acceleration equation, with time expressed in seconds is

$$\frac{d^2}{dt^2}(\theta_r) = \frac{1}{2H}(T_e - T_m) \tag{6.58}$$

where the electromagnetic torque is given by

$$T_e = E_d^{'} i_{ds} + E_q^{'} i_{qs} \tag{6.59}$$

and, the load torque can be expressed as,

$$T_m = T_0(\omega_r)^m \tag{6.60}$$

or

$$T_m = T_0(a\omega_r^2 + b\omega_r + c) \tag{6.61}$$

depending on the type of loads where $\omega_r = \frac{d}{dt}(\theta_r)$. Figure 6.14 shows the block diagram of the induction motor that is used in TSSP.

Load modeling itself is a very difficult task as meaningful data are simply unavailable and collecting and processing load data is expensive. Moreover, exact simulation of loads requires that at each time step, a load flow study be carried out in order to obtain the accurate bus voltage. This will increase the computation effort beyond an acceptable level. However, an alternative is to calculate a new operating point by a fast decoupled load flow program[6–7] only at the instant when an event or a disturbance happens. At other times, the bus voltage is held constant in load representations as computed in the latest load flow study.

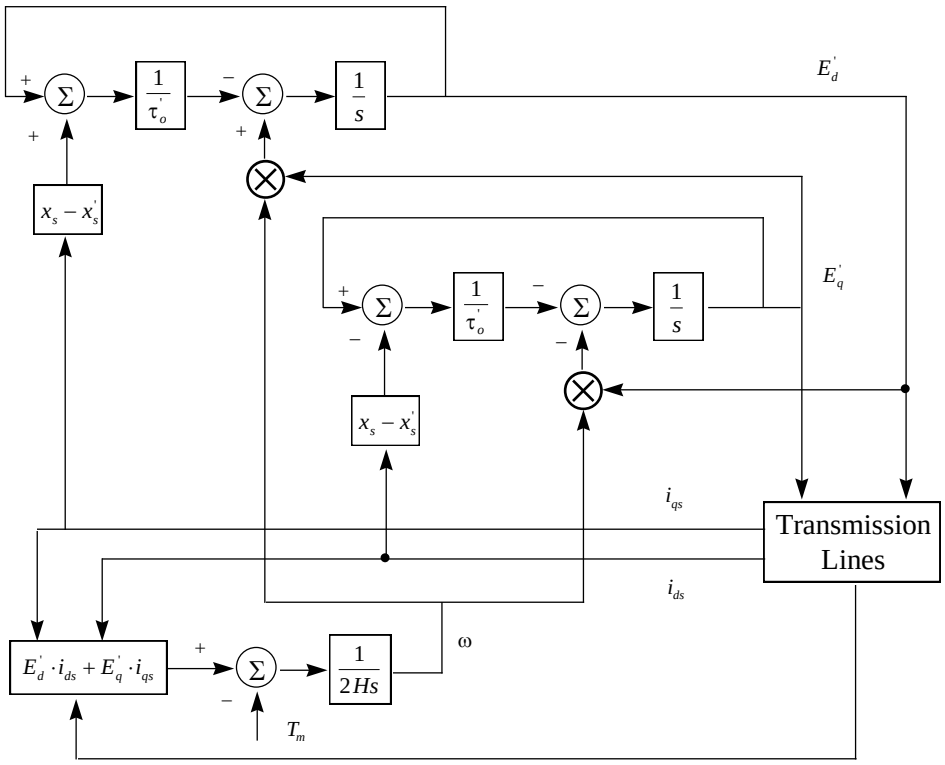

Fig. 6.14 Block Diagram of An Induction Motor

6.2.7 DC Transmission

An alternating current transmission system is represented by a positive–sequence circuit in transient stability simulations. In order to achieve high performance in power systems, direct current transmission system is used. It provides maximum flexibility in power control and enhances transient stability.

Figure 6.15 shows a schematic diagram of a direct current(DC) link between two AC transmission systems. The transformers provide an

ungrounded three–phase voltage source of appropriate level to the valve bridge of the rectifier/inverter. The DC line is similar to an AC line, except it has different numbers of conductors and spacing between conductors. Figure 6.16 is the corresponding equivalent circuit. The direct current flowing from the rectifier to the inverter is given by

$$I_d = \frac{V_{dor}\cos(\alpha) - V_{doi}\cos(\gamma)}{R_{cr} + R_L - R_{ci}} \tag{6.62}$$

where

α = the ignition delay angle,

γ = the excitation advance angle.

The power at the rectifier/inverter terminals is given by, respectively,

$$P_{dr} = V_{dr} + I_d \tag{6.63}$$

and

$$P_{di} = V_{di} I_d = P_{dr} - R_L I_d^2 \tag{6.64}$$

Figure 6.17 shows a schematic diagram of a converter. Let B be the number of bridges in series, T the transformer ratio. Then the ideal no–load voltage on the DC side is given by

$$V_{do} = \frac{3\sqrt{2}}{\pi} BTV_t \tag{6.65}$$

where V_t is the terminal voltage at the AC side.

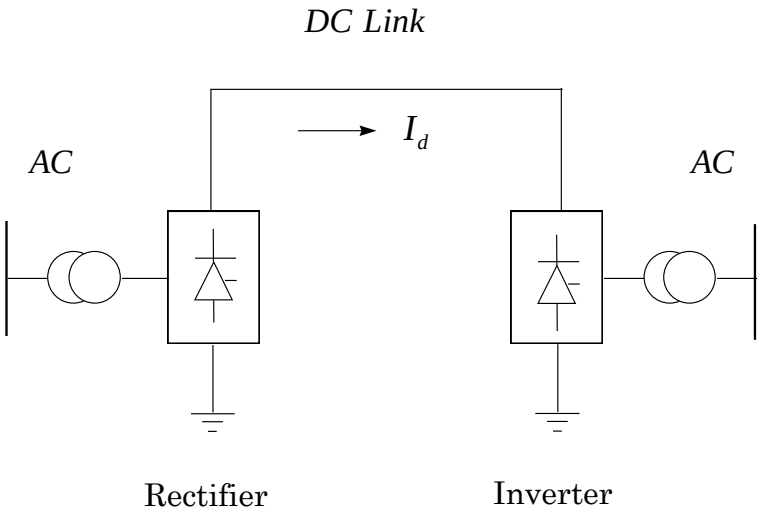

Fig. 6.15 Schematic Diagram of A DC Line

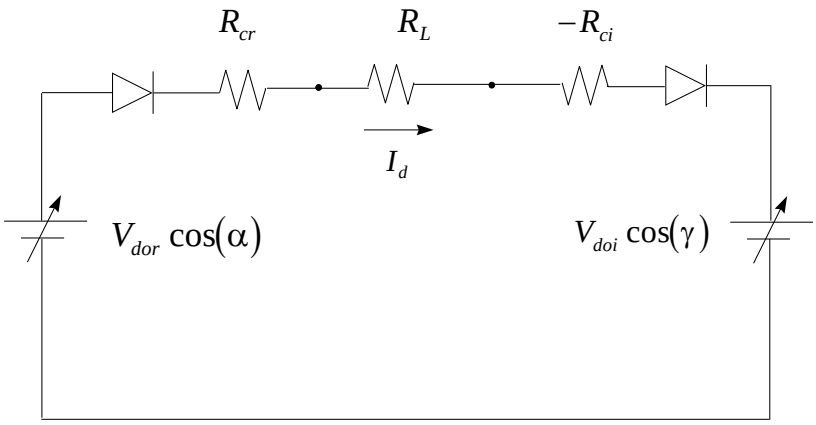

Fig. 6.16 Equivalent Circuit of A HVDC Link

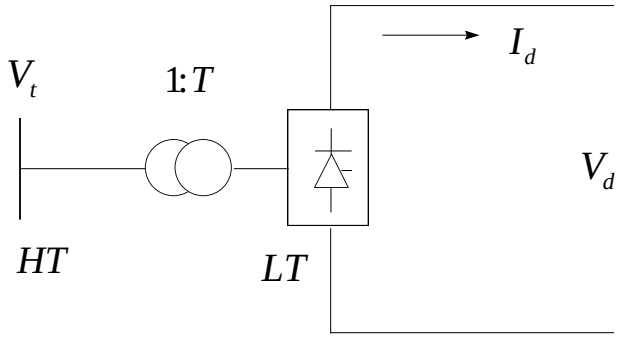

Fig. 6.17 Converter Representation

When there is load, there will be voltage drop across each bridge. Now the voltage on the DC side is expressed as one of the following two

$$V_d = V_{do}\cos(\alpha) - I_d B\left(\frac{3}{\pi}x_c\right) \tag{6.66}$$

$$V_d = V_{do}\cos(\gamma) - I_d B\left(\frac{3}{\pi}x_c\right) \tag{6.67}$$

where

$R_c = \frac{3}{\pi}wL_c$, the equivalent commutating resistance.

The power factor can be expressed as

$$\varsigma = \cos^{-1}\left(\frac{V_d}{V_{do}}\right) \tag{6.68}$$

$$P = V_d I_d \tag{6.69}$$

$$Q = P\tan(\varsigma) \tag{6.70}$$

where P, Q are active and reactive power, respectively.

For a more detailed representation of DC transmission system and its control for transient stability study, the reader is referred to [6–10]. This subject is further treated in Chapter 7 where TSSP in SIMULINK is presented.

6.3 SYSTEM DISTURBANCES

The modeling of system disturbances is an important aspect in simulating the dynamic behavior of a power system with acceptable accuracy. Both symmetrical and asymmetrical disturbances should be modeled. A symmetrical disturbance can be easily modeled as the system will remain symmetrical under such a disturbance. Under asymmetrical disturbances, the solution of the stability problem for the disturbed three–phase network can be carried out by a three–phase stability program, where the symmetrical component method is employed to resolve the system into three symmetrical three–phase systems. Therefore, the total computations will increase up to three times. On the other hand, it has been found [6–15] that the average braking torque produced by the reaction of the two magnetic fields (one produced by the negative sequence current and the other by the rotor winding current) is approximately zero, and that zero sequence currents yield a zero component torque as the three–phase zero sequence currents are electrically in phase and have 120 degree displacement in space. Therefore,

only the positive sequence quantities are needed to be taken into account during a transient process. However, the negative and zero sequence networks have to be incorporated into the positive sequence network at the fault point.

Each disturbance can be described and modeled as a sequence of events. They may include pre–fault, fault, post–fault and line restoration, i.e., autoreclosure if any, etc. The admittance matrix of the network is modified each time there is a change in the configuration of the network during the disturbance. As most faults in a practical power system are asymmetrical in nature, it is important to know what behavior a system would exhibit under such disturbances and what measures should be taken to maintain system stability while maximizing the availability of power supply to customers. Detailed modeling aspects will be further covered in Chapter 7 when presenting TSSP in SIMULINK environment.